Prepared for submission to JCAP

Spectral shape analysis for electron antineutrino oscillation study by using ^{8}Li generator with ^{252}Cf source

Jae Won Shin,[a] **Myung-Ki Cheoun,**[a,1] **Toshitaka Kajino** [b,c] **and Takehito Hayakawa**[d]

[a]Department of Physics, Soongsil University,
Seoul 156-743, Korea
[b]Division of Theoretical Astronomy, National Astronomical Observatory of Japan,
Mitaka, Tokyo 181-8588, Japan
[c]Department of Physics, Graduate School of Science, University of Tokyo,
Hongo, Bunkyo-ku, Tokyo 113-0033, Japan
[d]National Institute for Quantum and Radiological Science and Technology,
2-4 Shirakata, Tokai, Naka, Ibaraki 319-1106, Japan

E-mail: shine8199@skku.edu, cheoun@ssu.ac.kr, kajino@nao.ac.jp,
hayakawa.takehito@qst.go.jp

Abstract. Existence of hypothetical fourth neutrino, so-called sterile neutrino, is one of open issues in the particle and neutrino physics. This fourth neutrino is a candidate for explaining some anomalies reported in LSND, MiniBoone, reactor experiments, and gallium experiments. To search for the existence of the sterile neutrino, we report detailed analysis of a feasible experiment for short baseline electron antineutrino ($\bar{\nu}_e$) disappearance study, in which a $\bar{\nu}_e$ source from ^{8}Li generator is considered under non-accelerator system. For ^{8}Li production, we suggest to use ^{252}Cf source as an intense neutron emitter, by which one can produce ^{8}Li isotope through ^{7}Li(n,γ)^{8}Li reaction, effectively. Using the ^{8}Li generator, one does not need any accelerator or reactor facilities because the generator can be placed on any present and/or planned neutrino detectors as closely as possible. For the effect of the possible sterile neutrinos, we estimate expected neutrino flux and event rates from the neutrino source scheme, and show neutrino disappearance features and possible reaction rate changes by the sterile neutrino using the spectral shape analysis.

Keywords: Short baseline neutrino disappearance, Electron antineutrino source, Sterile neutrinos

[1]Corresponding author.

arXiv:1804.08225v1 [physics.ins-det] 23 Apr 2018

Contents

1 Introduction **1**

2 Methods **2**
- 2.1 Electron antineutrino sources from ^{8}Li generator under non-accelerator system 2
- 2.2 Proposed experimental setup 3
- 2.3 Detection of electron antineutrino with liquid-scintillator detector 4
- 2.4 Tested hypothetical models for the sterile neutrinos 4

3 Results **5**
- 3.1 ^{8}Li isotope yield in the generator 5
- 3.2 Background consideration 7
- 3.3 Spectral shape analysis for short baseline electron antineutrino disappearance studies 8

4 Summary **10**

1 Introduction

Since the first observation of neutrino oscillation phenomena was done in Homestake Experiments [1], many experiments (e.g. KamioKanDe [2] and SNO [3] facilities) had confirmed the neutrino oscillation phenomena and showed that the oscillation mechanism resolves the long-standing discrepancies among measured and/or theoretical solar neutrino flux, so-called solar neutrino problem.

There are 'somewhat similar' discrepancies or anomalies, similar to the solar neutrino problem, that were observed in LSND [4], MiniBoone [5], reactor antineutrino experiments [6] and gallium experiments [7] despite the knowledge that three flavor neutrinos oscillate. These observations naturally lead to the possible existence of hypothetical fourth neutrino, so-called sterile neutrinos (ν_s), which may mix with standard three active neutrinos and do not interact with other particles. For the ν_s search, many interesting studies with several neutrino sources such as ∼100 kCi of ^{144}Ce-^{144}Pr antineutrino generators [8, 9] and electron antineutrinos ($\bar{\nu}_e$) from ^{8}Li by using an accelerator-based IsoDAR concept [10, 11], etc. have been proposed.

In the previous work, for the ν_s search, we proposed a fissionable isotope of ^{252}Cf as a radioactive isotope-based $\bar{\nu}_e$ production scheme [12]. With ^{252}Cf radioactive isotope, 99.99% enriched ^{7}Li and graphite, ^{8}Li isotopes as a $\bar{\nu}_e$ source can be produced effectively. ^{252}Cf emits neutrons with an average energy of approximately 2 MeV, and the generated neutron can produce ^{8}Li isotopes by the neutron capture reaction to ^{7}Li. Furthermore, ^{8}Li generator can be placed on existing and/or planned any neutrino detectors such as Borexino, JUNO, KamLAND, LENA and SNO+, etc. because one does not need any accelerator or reactor systems.

In this work, we study the experimental method by using spectral shape analysis with the neutrino source from the ^{8}Li generator based on a ^{252}Cf neutron source. Spectral shapes of the measured neutrinos can be analyzed independently of absolute flux values and give valuable chances to study the existence of fourth neutrinos. To decipher the effect of possible

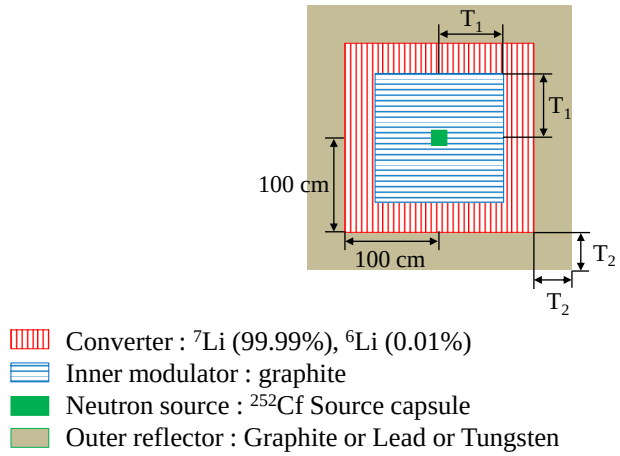


Figure 1. (Color online) A schematic cross section view showing cylindrical ^{8}Li generator.

sterile neutrinos from the shape analysis exploited in Daya Bay [13], Double Chooz [14], and RENO [15, 16] experiments, we calculate expected neutrino flux and event rates, and discuss neutrino disappearance features and possible reaction rate changes by the sterile neutrino. To simulate the non-accelerator ^{8}Li generator, we use particle transport Monte Carlo code, GEANT4 [17, 18].

2 Methods

2.1 Electron antineutrino sources from ^{8}Li generator under non-accelerator system

As an intense neutron emitter to generate ^{8}Li, we consider a ^{252}Cf isotope with a half-life ($T_{1/2}$) of 2.64 yr, which emits neutrons through spontaneous fission process. The following energy distribution of the neutron from ^{252}Cf known as Watt fission spectrum [19–21], $f(E) = \exp(-\frac{E}{1.025})\sinh(2.926E)^{1/2}$ is adopted, where E is the neutron energy in MeV, and the neutron emission rate of 2.34×10^{12} neutrons per second (n/s) for 1 g of ^{252}Cf is used in our work. These neutrons can produce ^{8}Li isotope through ^{7}Li(n,γ)^{8}Li reaction where the ^{8}Li becomes electron antineutrino source.

Figure 1 shows the ^{8}Li generator comprising 99.99% enhanced ^{7}Li convertor, ^{252}Cf source surrounded by the graphite modulator, and reflector materials such as C, Pb, W which wrap outside the Li convertor. The Li convertor has a cylindrical shape of a radius 100 cm and a length 200 cm, whose shape and size are based on the analysis performed in Ref. [11]. We place graphite as an neutron modulator in the ^{7}Li convertor. The graphite is usually preferred as a modulator (or reflector) due to its low absorption cross section and high

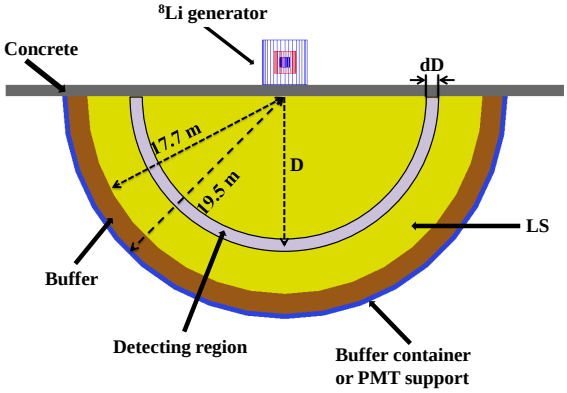


Figure 2. (Color online) Simulation geometry for hemisphere shape detector with ^{8}Li generator.

elastic scattering cross section for neutron.[1] With the graphite modulator, we can increase the production yield of ^{8}Li even though amounts of the ^{7}Li are less than those without graphite.

Heat production of the source can be issued for the experimental setup. Heat production of approximately 50 kCi of ^{144}Ce-^{144}Pr antineutrino generators and electron antineutrinos ($\bar{\nu}_e$) from ^{8}Li by using an accelerator-based IsoDAR concept are ~370 W and 600 kW, respectively. In contrast, the heat of a ^{252}Cf source with 1.0 g is approximately 38.5 W (decay heat of α-decay and spontaneous fission are 18.8 W/g and 19.7 W/g, respectively). This is much smaller than those from the above generators, and thus the cooling of 38.7 W is more easy. Also, in our design, because the ^{252}Cf source inside of the graphite and the detector can be located apart, the cooling of the neutrino source is more easy, if needed.

To calculate production rates of ^{8}Li by neutrons from ^{252}Cf, the GEANT4 (GEometry ANd Tracking) code [17, 18] is used. For an accurate simulation of neutron interactions, high precision models (G4HP) with G4Neutron Data Library (G4NDL) 4.5 are used in the present work, where the G4HP include cross sections and final states information for elastic, inelastic scattering, capture, fission, and isotope production. The data in G4NDL 4.5 come largely from the Evaluated Nuclear Data File (ENDF/B-VII) library [26].[2] ^{8}Li with $T_{1/2}$ of 0.838 s emits $\bar{\nu}_e$ through β^- decay, $^8\mathrm{Li} \rightarrow {}^8\mathrm{Be} + e^- + \bar{\nu}_e$. The energy distribution of the electron anti-neutrinos from ^{8}Li is calculated by using "G4RadioactiveDecay" [27, 28] class based on the Evaluated Nuclear Structure Data File (ENSDF) [29].

2.2 Proposed experimental setup

To study spectral shape analysis for the ν_s existence, a hemisphere shape liquid scintillator detector based on the JUNO [30] is considered. Figure 2 shows the simulation geometry for hemisphere shape detector with the ^{8}Li generator where D and dD mean the distance between the bottom of the plate and the center of the detection shell and the thickness of

[1] This concept known as the Adiabatic Resonance Crossing (ARC) was first proposed by Nobel Laureate Carlo Rubia [22] for the transmutation of long-lived nuclear waste and the medical radioisotope production [23–25].

[2] ENDF/B-VII library is developed and maintained by the Cross Section Evaluation Working Group (CSEWG) where the data are based on experimental and theoretical data.

the shell, respectively. In this work, we consider a hemisphere shape of LS detectors with a radius of 17.7 m where the target proton number (n_p) in the detector is 0.725×10^{33} (approximately 10 kt) [30]. The expected event rate is obtained within the detecting region of LS detectors for various D values with the cylindrical ^{8}Li generator.

2.3 Detection of electron antineutrino with liquid-scintillator detector

For detection of electron antineutrinos, an inverse beta decay (IBD) reaction, $\bar{\nu}_e + p \rightarrow e^+ + n$, is considered. The IBD reaction gives two distinct signals in electron anti-neutrino detections; one is the prompt signal due to an annihilation of a positron, and another is a delayed signal of a 2.2 MeV γ-ray via neutron capture. The event rate ($ER^{IBD}_{\bar{\nu}_e}$) for IBD can be written as

$$ER^{IBD}_{\bar{\nu}_e} = n_p \int_{E_{th}}^{E_{max}} dE_{\bar{\nu}} \Phi_{\bar{\nu}_e}(E_{\bar{\nu}}) \mathrm{P}_{\nu\bar{\nu}}(E_{\bar{\nu}}) \sigma^{IBD}_{\bar{\nu}_e}(E_{\bar{\nu}_e}) \ , \tag{2.1}$$

where n_p is the number of target protons within the fiducial volume of detector. $\Phi_{\bar{\nu}_e}(E_{\bar{\nu}})$ is the electron-antineutrino flux from ^{8}Li, E_{max} is the maximal neutrino energy, E_{th} is the threshold energy of the reaction, $\mathrm{P}_{\nu\bar{\nu}}(E_{\bar{\nu}})$ is an energy dependent electron-antineutrino survival probability, and $E_{\bar{\nu}}$ is energy of the incident antineutrino. The energy dependent cross section of the IBD in Eq. (2.1) can be expressed by [31, 32]

$$\sigma^{IBD}_{\bar{\nu}_e}(E_{\bar{\nu}_e}) \approx p_e E_e E_{\bar{\nu}_e}^{-0.07056+0.02018\ln E_{\bar{\nu}_e} - 0.001953\ln^3 E_{\bar{\nu}_e}} \times 10^{-43}[\mathrm{cm}^2], \tag{2.2}$$

where p_e, E_e and $E_{\bar{\nu}_e}$ are the positron momentum, total energy of the positron and the energy of $\bar{\nu}_e$ in MeV, respectively. $E_e = E_{\bar{\nu}_e} - \Delta$ where Δ is mass difference between m_n and m_p ($\Delta = m_n - m_p \approx 1.293$ MeV). This cross section agrees within few per-mille with the full calculation including the radiative corrections and the final-state interactions in IBD.[3]

2.4 Tested hypothetical models for the sterile neutrinos

By using our $\bar{\nu}_e$ source, we can study the possible existence of the fourth neutrino, sterile neutrino. For three neutrino oscillation model, we use $\mathrm{P}_{\nu\bar{\nu}}(E_{\bar{\nu}})$ ($\equiv \mathrm{P}_3$) given by [33]

$$P_3 = 1 - \sin^2 2\theta_{13} S_{23} - c^4_{13} \sin^2 2\theta_{12} S_{12}, \tag{2.3}$$

where $S_{23} = \sin^2(\Delta m^2_{32} L/4E)$ and $S_{12} = \sin^2(\Delta m^2_{21} L/4E)$. L and E mean the source to detector distance and the neutrino energy, respectively. Neutrino oscillation parameters in Eq. (2.3) are taken from a global fit from Ref. [34].

To see the ν_s effect, we also use electron-antineutrino survival probabilities in the 3+1 and 3+2 models where the survival probabilities can be written as [11]

$$P_{3+1} = 1 - 4|U_{e4}|^2(1 - |U_{e4}|^2)\sin^2(\Delta m^2_{41} L/4E), \tag{2.4}$$

$$\begin{aligned} P_{3+2} = 1 \ &- \ 4[(1 - |U_{e4}|^2 - |U_{e5}|^2) \\ &\times (|U_{e4}|^2 \sin^2(\Delta m^2_{41} L/4E) + |U_{e5}|^2 \sin^2(\Delta m^2_{51} L/4E)) \\ &+ \ |U_{e4}|^2 |U_{e5}|^2 \sin^2(\Delta m^2_{54} L/4E)]. \end{aligned} \tag{2.5}$$

[3] There is another possible $\bar{\nu}_e$ detection channel, $\bar{\nu}_e$-e$^-$ elastic scattering (ES). Through the $\bar{\nu}_e$-e$^-$ ES, antineutrinos can be indirectly measured by the outgoing scattered electron which can be identified by means of the scintillation light produced in the liquid-scintillator (LS). But, reaction rates for the ES are much smaller than those for IBD. Therefore, we only consider IBD reaction for the following neutrino disappearance study.

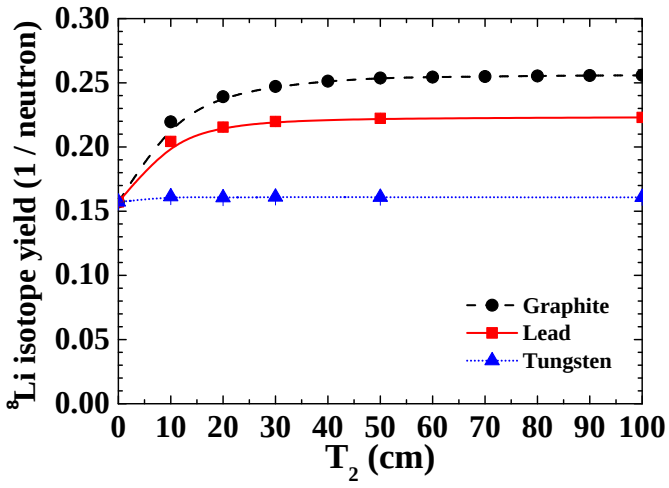


Figure 3. (Color online) ^{8}Li isotope yields for graphite, lead and tungsten with respect to T_2. T_1 is set to 43 cm because the value is optimal thickness. The filled circles, squares and triangles denote results for graphite, lead and tungsten, respectively.

The oscillation parameters for the 3+1 model in Eq. (2.4) and for the 3+2 model in Eq. (2.5) are taken from the best-fit points from the combined short base lines (SBL) and IceCube data set [35], and reactor antineutrino data [36], respectively.

3 Results

3.1 ^{8}Li isotope yield in the generator

First, we calculate the production yield of ^{8}Li with the ^{252}Cf source coupled only with the Li convertor. Yield of 0.0045 ^{8}Li per neutron (^{8}Li/n) is obtained because neutrons can easily escape from the convertor, so that they are not effectively captured by ^{7}Li isotopes. When graphite material, the inner modulator in Fig. 1, is placed in the Li convertor, ^{8}Li yield can be increased compared to that without the graphite. As the graphite thickness increases, numbers of the collisions between the neutron and the carbon nuclei also increase. Consequently, capture probability of the neutron by ^{7}Li can also increase. If the graphite is too thick, however, it becomes hard for the scattered neutron to escape from the graphite. We found that yields of ^{8}Li increase when T_1 increases up to 43 cm. As the T_1 of the inner modulator increases more than 43 cm, yields of ^{8}Li decrease. Maximum yield of ^{8}Li turns out to be 0.1572 ^{8}Li/n at $T_1 = 43$ cm, whose yield is about 35 times larger than that without graphite.

To further increase the yields of ^{8}Li, outer reflector with the thickness T_2 in Fig. 1 is considered to be located out of the Li convertor. The production yield for ^{8}Li with respect to T_2 is plotted in Fig. 3 where the optimal thickness of T_1 is chosen as 43 cm. As the reflector materials, graphite, lead and tungsten are considered. For graphite, ^{8}Li yields increase up to 0.256 ^{8}Li/n as the T_2 increases. With the T_2 larger than 50 cm, yields for ^{8}Li are almost saturated. Results for lead and tungsten as the T_2 material are also shown in Fig. 3. The production yields of ^{8}Li for lead and tungsten increase up to 0.22 and 0.16 ^{8}Li/n, respectively,

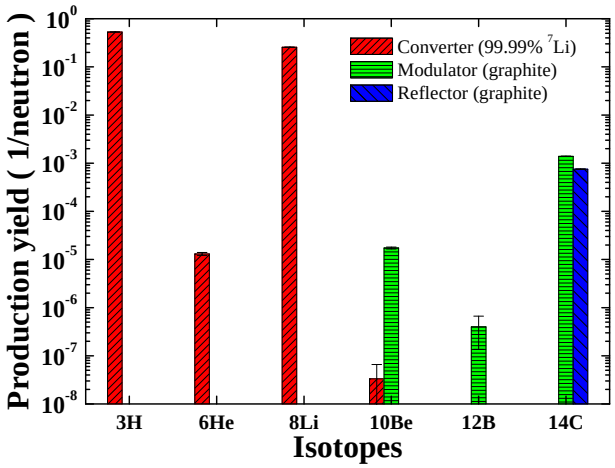


Figure 4. (Color online) Production yields of unstable isotopes in the ^{8}Li generator. The modulator and the reflector materials are chosen as graphite, and T_1 and T_2 are 43 cm and 100 cm, respectively.

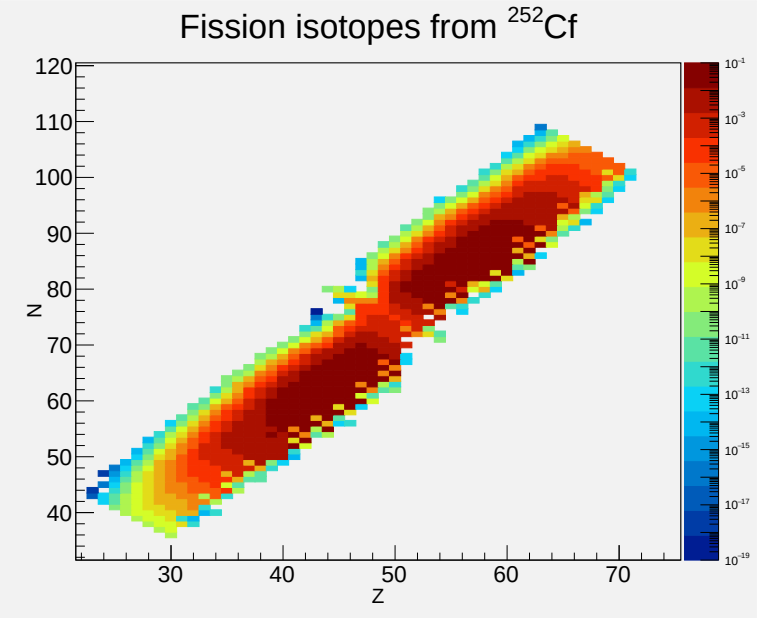


Figure 5. (Color online) Yields of fission isotopes from ^{252}Cf.

with the increase of the T_2. Yields of ^{8}Li for lead and tungsten as the T_2 material are smaller than that of graphite by $\sim 16\%$ and $\sim 60\%$, respectively. It is found that yield of 0.256 ^{8}Li/n is obtained with both the two graphite materials (modulator and reflector). Therefore, we use this value for the setup in this work.

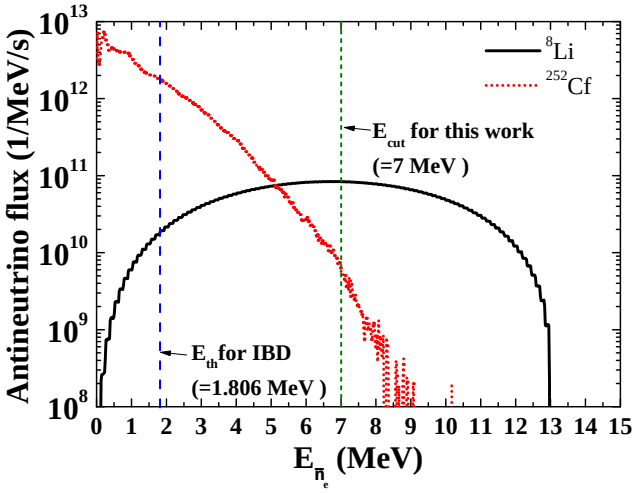


Figure 6. (Color online) $\bar{\nu}_e$ flux from ^{8}Li and fission products of ^{252}Cf. The black solid lines denote the electron-antineutrino from ^{8}Li and the red dotted lines represent those from fission products of ^{252}Cf.

3.2 Background consideration

The IBD reactions provide two distinct signals in electron anti-neutrino detection; one is the prompt signal due to an annihilation of a positron, and another is a delayed signal of a 2.2 MeV γ via a neutron capture that provides almost unambiguous antineutrino event detection. These coincident features give an efficient rejection of other possible backgrounds.

In fact, various unstable isotopes can be produced in both Li convertor and graphite modulator and reflectors, and emit antineutrinos. Thus they can affect the neutrino detection. Production yields of unstable isotopes for $T_1 = 43$ cm and $T_2 = 100$ cm are plotted in Fig. 4. Figure 4 shows that ^{3}H, ^{6}He and ^{10}Be are produced as well as ^{8}Li in Li convertor. However, ^{3}H has a long half-life of ∼12.3 y. Also, production yields of ^{6}He and ^{10}Be are much lower compared to those of ^{8}Li by factors ∼10^4 and ∼10^7, respectively. Other unstable isotopes, ^{10}Be, ^{12}B and ^{14}C, are also produced in graphite materials. Because of very low yields for ^{10}Be and ^{12}B and a long half-life of ^{14}C (∼5.7×10^3 y), their contributions are marginal for the IBD neutrino detections.[4]

Background neutrinos such as neutrinos from fission product of ^{252}Cf (ν_f) and geo-neutrinos ($\nu_{geo.}$) can also affect the neutrino detection. To check the ν_f effect, we evaluate flux and event rate for ν_f by using ENDF/B-VII.1 and ENSDF data. Figure 5 shows the yields of fission products from ^{252}Cf isotope where the yield data of 1245 isotopes in the region with $30 < Z < 70$ and $40 < N < 110$ are taken from ENDF/B-VII.1.

First, we estimate the ν_f flux by using ENSDF data. In our estimation, we assume that unstable isotopes (880 isotopes) are fully decay with half-lifes shorter than 1 yr. Figure 6 shows electron antineutrino flux from ^{252}Cf and the flux from ^{8}Li. In the figure, the ν_f

[4]For lead and tungsten as a reflector material, ^{205,209}Pb and ^{181,185,187}W isotopes are produced. But, ^{205}Pb has a long half-life of ∼1.73×10^7 y, and ^{181}W emits low energy electron neutrinos (Q = 0.188 MeV), but does not electron antineutrinos. And the $\bar{\nu}_e$ from ^{209}Pb (Q = 0.644 MeV), ^{185}W (Q = 0.432 MeV) and ^{187}W (Q = 1.31 MeV) have the endpoint energies less than the IBD reaction threshold (1.806 MeV). Therefore, they do not affect the main IBD reaction.

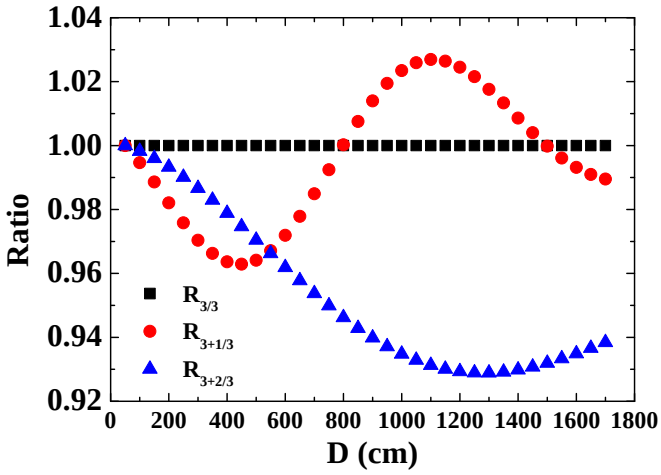


Figure 7. (Color online) The event ratios ER_3, ER_{3+1} and ER_{3+2} of ER_3 with respect to D.

is dominant in the low energy region below the IBD reaction threshold compared with the flux from ^{8}Li. However, in the energy region of $E_{\bar{\nu}_e} > 5.1$ MeV, the neutrino flux from ^{8}Li becomes larger than ν_f flux. It is also found that total event ratios by the neutrino from ^{8}Li ($\nu_{^8Li}$) for $E_{\bar{\nu}_e} > 7$ MeV is larger than those from ν_f by three orders of magnitudes and thus contributions of the ν_f are negligible compare to the $\nu_{^8Li}$. Consequently, we can remove the ν_f effect with the neutrino energy cut of 7 MeV in this work.

Geo-neutrinos, which can affect the neutrino detectors, are produced via β-decays of long-lived radioactive isotopes such as ^{40}K, ^{238}U and ^{232}Th that are present in the Earth. ^{40}K isotopes decay into ^{40}Ca isotopes (branching ratio = 89.14%) through β^--decays with the Q value of 1.311 MeV and thus emit electron antineutrinos. However, the neutrinos, which have the maximum energy near to the Q value, cannot affect the IBD reaction because of a kinematic threshold of 1.806 MeV for the IBD. Numbers of unstable isotopes are generated in the chains of ^{238}U and ^{232}Th. KamLAND [37] and Borexino [38, 39] have measured a rate for $\nu_{geo.}$ ($\sim$ a few events/(100 ton $\cdot$ yr)) due to the decay of U or Th in the Earth. The end points of the neutrino energy spectrum from ^{232}Th and ^{238}U chain are about 2.25 MeV and 3.3 MeV, respectively. In this work, we use the neutrino energy cut of 7 MeV. Therefore, contributions of the $\nu_{geo.}$ are also negligible compared to those of $\bar{\nu}_e$ from ^{8}Li ($\nu_{^8Li}$).

Other radiations such as neutrons and gammas can affect detection for neutrinos. But, by using a ^{252}Cf source with a low intensity and small detectors (for neutrons and gammas detections), we can measure the background radiations from the setup suggested in this work.

3.3 Spectral shape analysis for short baseline electron antineutrino disappearance studies

In order to see the effect by the sterile neutrinos, we consider ^{8}Li generator and hemisphere shape LS detector based on the JUNO [30], as explained in Fig. 2. The expected event rates under P_3 model are compared with the P_{3+1} and the P_{3+2} models, and distinct features for each model are obtained. Figure 7 shows results for the expected total event ratios (ERs) of P_3, P_{3+1} and P_{3+2} to P_3 as a function of D, which is the distance between bottom of the

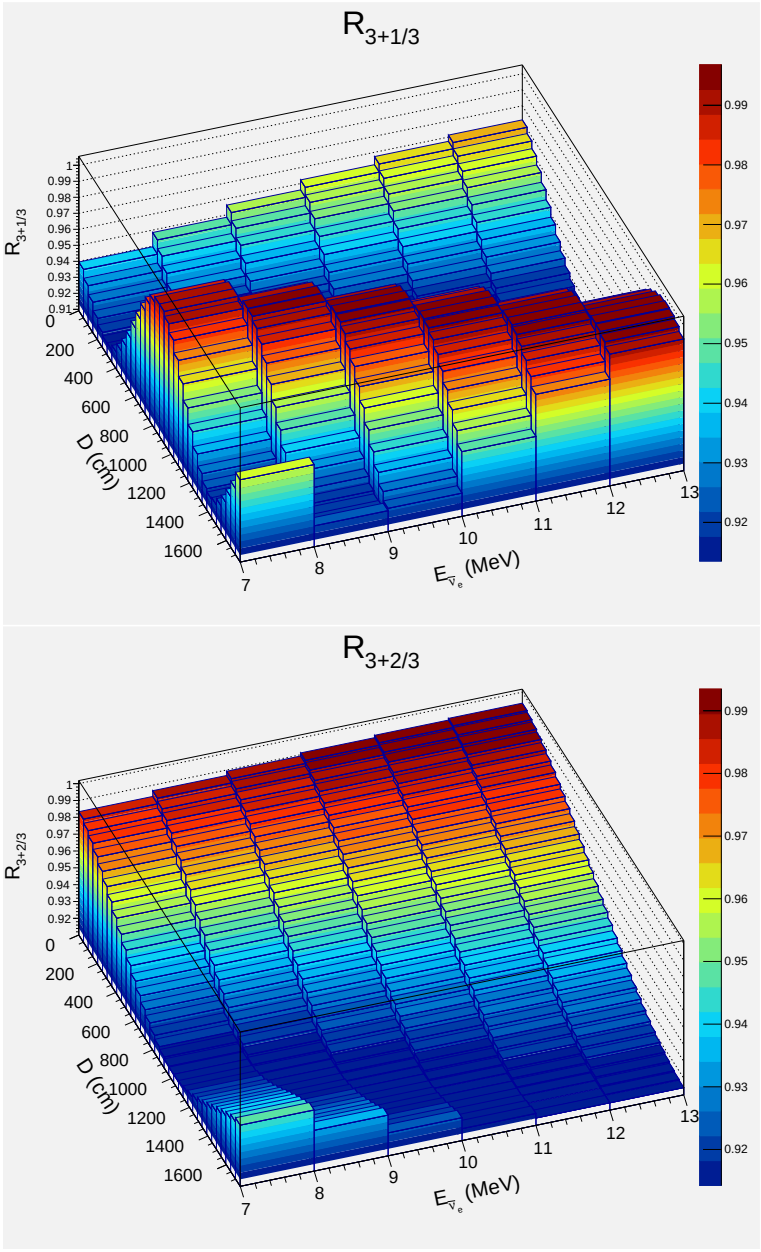


Figure 8. (Color online) $\bar{\nu}_e$ energy distribution of $R_{3+1/3}$ and $R_{3+2/3}$ with respect to D.

plate and center of the shell for detection in Fig. 2. $R_{3/3}$ ($R_{3+1/3}$ and $R_{3+2/3}$) means the ratio ER_3 (ER_{3+1} and ER_{3+2}) to ER_3. If there are no sterile neutrinos, the ratio should be 1 in Fig. 7.

Under the 3+1 sterile neutrino scenario with the best fit parameter, however, oscillation shape is largely deviated from the unit number 1. The minimum and the maximum are shown at D = 450 cm and D = 1100 cm, respectively. For the 3+2 scenario, the ratio decreases for D < 1200 cm with the D increase, and the period of the oscillation is found to be much longer than that of the 3+1 scenario. At D = 1100 cm, the minimum for the 3+2 scenario and the 3+1 scenario maximum appear clearly. The neutrino energy distributions for different D

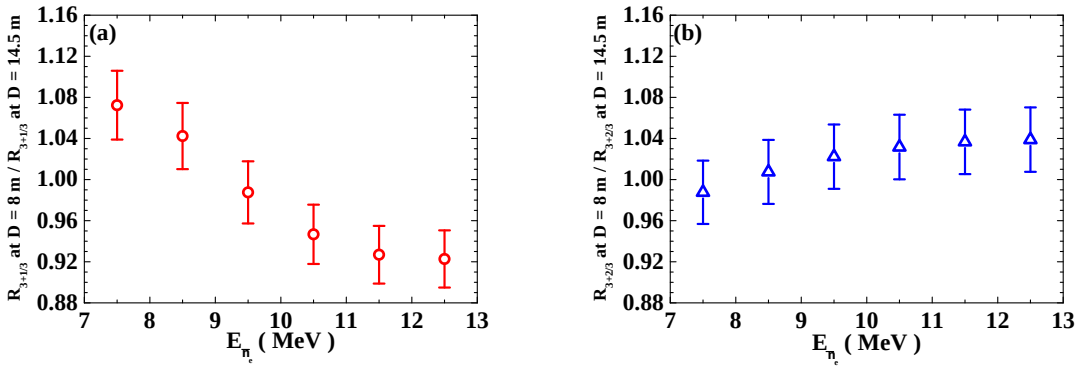


Figure 9. (Color online) Panel (a) is the expected ratio of $R_{3+1/3}$ at D = 8 m and D = 14.5 m with respect to $E_{\bar{\nu}_e}$. Panel (b) is for $R_{3+2/3}$ case.

values with dD = 1 m are shown in Fig. 8. It is found that the energy oscillation shapes are also varying as the D changes.

For the $R_{3+1/3}$ ratio in the figure, the peak positions of neutrino energies increase as the D increase. On the contrary, monotonic changes in the shapes show up for $R_{3+2/3}$ ratio in our setup. More drastic changes for the 3+1 sterile neutrino scenario can be obtained from two distinct signals at two different detector positions, at D = 8 m and D = 14.5 m. For D = 8 m, $R_{3+1/3}$ ratios are 0.917 and 0.988 at $E_{\bar{\nu}_e}$ = 12.5 MeV and $E_{\bar{\nu}_e}$ = 7.5 MeV, respectively. However, for D = 14.5 m, the situation is reversed. That is, $R_{3+1/3}$ ratios of 0.994 and 0.922 are obtained at $E_{\bar{\nu}_e}$ = 12.5 MeV and $E_{\bar{\nu}_e}$ = 7.5 MeV, respectively. Therefore, using the expected two different signals for D = 8 m and D = 14.5 m, we can easily search for 3+1 sterile neutrino scenario. Figure 9 shows the expected ratio of $R_{3+1/3}$ at D = 8 m and D = 14.5 m in panel (a), and that of $R_{3+2/3}$ is shown in panel (b).

For the error bars in the analysis, we assumed a statistical error of 2%, a systematic error of 2%, an energy resolution of $3\%/\sqrt{E/MeV}$, a position resolution of 12 cm, and a IBD cross section error of 0.5%. Decrease pattern can be seen clearly in the Fig. 9 (a) as the $E_{\bar{\nu}_e}$ increase. Also, the maximum and the minimum values of the ratios are 1.07 at $E_{\bar{\nu}_e}$ = 7.5 MeV and 0.92 at $E_{\bar{\nu}_e}$ = 12.5 MeV, respectively. If we can measure approximately 15% deviation from the expected events, we can find a clue to the problem of whether the P_{3+1} model is the most appropriate scenario.

4 Summary

In this work, we propose an experimental setup for neutrino spectral shape analysis by using a ^{8}Li generator under non-accelerator system. Unstable isotope, ^{8}Li, emits $\bar{\nu}_e$ having energy range $0 < E_{\bar{\nu}_e} < 13$ MeV ($< E_{\bar{\nu}_e} > \sim 7$ MeV) through β^- decay where the ^{8}Li is produced via ^{7}Li(n,γ)^{8}Li reaction with an intense neutron emitter, ^{252}Cf. The ^{8}Li generator suggested in our scheme can be placed and applied to any neutrino detectors such as Borexino, JUNO, KamLAND, LENA and SNO+, because accelerator or reactor systems are not needed anymore.

Suggested ^{8}Li generator is very compact, so that neutrino detectors can be placed within a few meters from the neutrino source with $E_{\bar{\nu}_e} < 13$ MeV. Moreover neutrinos from the

source can be so effectively controlled. Consequently, background neutrinos can be exactly separated as mentioned in Sec. 3.2. It means that our scheme could be a very efficient neutrino source for the study of 1 eV mass scale sterile neutrino as well as other neutrino oscillation studies.

The expected event rates with P_3, P_{3+1} and P_{3+2} models with best fit points, and their ratios are presented for different detector distances. Our results show that neutrino disappearance features and possible reaction rate are changed significantly by the sterile neutrino. These distinct features can give useful chances to search for the existence of a sterile neutrino as well as the test of the 3+1 or 3+2 sterile neutrinos scenarios. In particular, if we can confirm 15% deviation in Fig. 9, we can conclude whether P_{3+1} model is the most appropriate sterile neutrino model or not.

Acknowledgments

The work of J. W. Shin is supported by the National Research Foundation of Korea (Grant No. NRF-2015R1C1A1A01054083), the work of M.-K. Cheoun is supported by the National Research Foundation of Korea (Grant No. NRF-2015K2A9A1A06046598 and NRF-2017R1E1A1A01074023).

References

[1] R. Davis, D. S. Harmer and K. C. Hoffman, *Search for Neutrinos from the Sun*, *Phys. Rev. Lett.* **20** (1968) 1205–1209.

[2] K. Abe et al., *Solar neutrino results in Super-Kamiokande-III*, *Phys. Rev. D* **83** (2011) 052010.

[3] B. Aharmim et al., *Combined analysis of all three phases of solar neutrino data from the Sudbury Neutrino Observatory*, *Phys. Rev. C* **88** (2013) 025501.

[4] A. Aguilar-Arevalo and others (LSND collaboration), *Evidence for neutrino oscillations from the observation of $\bar{\nu}_e$ appearance in a $\bar{\nu}_\mu$ beam*, *Phys. Rev. D* **64** (2001) 112007.

[5] A. Aguilar-Arevalo and others (MiniBooNE Collaboration), *Event excess in the MiniBooNE search for $\bar{\nu}_\mu \to \bar{\nu}_e$ oscillations*, *Phys. Rev. Lett.* **105** (2010) 181801.

[6] G. Mention, M. Fechner, T. Lasserre, T. A. Mueller, D. Lhuillier, M. Cribier et al., *Reactor antineutrino anomaly*, *Phys. Rev. D* **83** (2011) 073006.

[7] C. Giunti and M. Laveder, *Statistical significance of the gallium anomaly*, *Phys. Rev. C* **83** (2011) 065504.

[8] A. Gando and others, *CeLAND: search for a 4th light neutrino state with a 3 PBq 144Ce-144Pr electron antineutrino generator in KamLAND*, 2013.

[9] G. Bellini et al., *SOX: Short distance neutrino Oscillations with BoreXino*, *JHEP* **2013** (2013) 38.

[10] L. A. Mikaelian, P. E. Spivak and V. G. Tsinoyev, *A proposal for experiments in low-energy antineutrino physics*, *Nucl. Phys.* **70** (1965) 574–576.

[11] A. Bungau, A. Adelmann, J. R. Alonso, W. Barletta, R. Barlow, L. Bartoszek et al., *Proposal for an Electron Antineutrino Disappearance Search Using High-Rate ^{8}Li Production and Decay*, *Phys. Rev. Lett.* **109** (2012) 141802.

[12] J. W. Shin, M.-K. Cheoun, T. Kajino and T. Hayakawa, *A new scheme for short baseline electron antineutrino disappearance study*, *J. Phys. G: Nucl. Part. Phys.* **44** (2017) 09LT01.

[13] F. P. An and others (Daya Bay Collaboration), *Measurement of the Reactor Antineutrino Flux and Spectrum at Daya Bay*, *Phys. Rev. Lett.* **116** (2016) 061801.

[14] Y. Abe et al., *Improved measurements of the neutrino mixing angle θ_{13} with the Double Chooz detector*, *JHEP* **2014** (2014) 086.

[15] S.-B. Kim, *Observation of Reactor Electron Antineutrino Disappearance at RENO*, *Nucl. Phys. B Proc. Suppl.* **235–236** (2013) 24–29.

[16] S.-H. Seo, *New Results from RENO and The 5 MeV Excess*, *AIP Conf. Proc.* **1666** (2015) 080002.

[17] S. Agostinelli et al., *GEANT4—a simulation toolkit*, *Nucl. Instrum. Meth. A* **506** (2003) 250–303.

[18] J. Allison et al., *Geant4 developments and applications*, *IEEE Trans. Nucl. Sci.* **53** (2006) 270–278.

[19] B. E. Watt, *Energy Spectrum of Neutrons from Thermal Fission of U^{235}*, *Phys. Rev.* **87** (1952) 1037.

[20] A. B. Smith, P. R. Fields and J. H. Roberts, *Spontaneous Fission Neutron Spectrum of Cf^{252}*, *Phys. Rev.* **108** (1957) 411.

[21] X-5 MONTE CARLO TEAM, *MCNP-A General Monte Carlo N-Particle Transport Code, Version 5*, 2003.

[22] C. Rubbia, *Resonance enhanced neutron captures for element activation and waste transmutation.*, 1997.

[23] P. Froment, I. Tilquin, M. Cogneau, T. Delbar, J. Vervier and G. Ryckewaert, *The production of radioisotopes for medical applications by the adiabatic resonance crossing (ARC) technique*, *Nucl. Instrum. Meth. A* **493** (2002) 165–175.

[24] K. Abbas, S. Buono, N. Burgio, G. Cotogno, N. Gibson, L. Maciocco et al., *Development of an accelerator driven neutron activator for medical radioisotope production*, *Nucl. Instrum. Meth. A* **601** (2009) 223–228.

[25] A. Khorshidi, M. Sadeghi, A. Pazirandeh, C. Tenreiro and Y. Kadi, *Radioanalytical prediction of radiative capture in ^{99}Mo production via transmutation adiabatic resonance crossing by cyclotron*, *J. Radioanal Nucl. Chem.* **299** (2014) 303–310.

[26] "ENDF/B-VII.1."

[27] P. Truscott, *Treatment of Radioactive Decay in Geant4*, *Tech. Rep. Qinetiq* **60** (2002) 2966–2983.

[28] S. Hauf, M. Kuster, M. Batič, Z. W. Bell, D. H. H. Hoffmann, P. M. Lang et al., *Radioactive Decays in Geant4*, *IEEE Trans. Nucl. Sci.* **60** (2013) 2966–2983.

[29] *ENSDF*, 2015.

[30] F. An et al., *Neutrino physics with JUNO*, *J. Phys. G* **43** (2016) 030401.

[31] R. Möllenberg, *Monte Carlo study of solar ^8B neutrinos and the diffuse supernova neutrino background in LENA*. PhD dissertation, Technische Universitat, Munchen, June-Aug., 2013.

[32] A. Strumia and F. Vissani, *Precise quasielastic neutrino/nucleon cross-section*, *Phys. Lett. B* **564** (2003) 42–54.

[33] A. Strumia and F. Vissani, *Neutrino masses and mixings and ...*, 2010.

[34] M. C. Gonzalez-Garcia, M. Maltoni, J. Salvado and T. Schwetz, *Global fit to three neutrino mixing: critical look at present precision*, *JHEP* **2012** (2012) 123.

[35] G. H. Collin, C. A. Arg'uelles, J. M. Conrad and M. H. Shaevitz, *First Constraints on the Complete Neutrino Mixing Matrix with a Sterile Neutrino*, *Phys. Rev. Lett.* **117** (2016) 221801, [1607.00011].

[36] J. Kopp, M. Maltoni and T. Schwetz, *Are There Sterile Neutrinos at the eV Scale?*, *Phys. Rev. Lett.* **107** (2011) 091801.

[37] K. Inoue, 2010.

[38] G. Bellini and others (Borexino Collaboration), *Observation of geo-neutrinos*, *Phys. Lett. B* **687** (2010) 299–304.

[39] G. Bellini and others (Borexino Collaboration), *Measurement of geo-neutrinos from 1353 days of Borexino*, *Phys. Lett. B* **722** (2013) 295–300.